Quantum Chemical Modeling of the Full Catalytic Cycle for Selective Oxidation of Propane to Propene on the M1 Phase of Mo−Te−Nb−O Mixed-Metal Oxide Catalysts

Karnajit Sen,* Ansgar Schäfer, Frank Rosowski, Dmitry I. Sharapa, and Felix Studt*

ABSTRACT: In this work, we have performed a quantum chemical study for the selective oxidation of propane to propene on the M1 phase of a mixed-metal oxide catalyst, consisting of Mo−Nb−T e−O. T he M1 phase of the catalyst has a complex surface structure that involves different arrangements of metal oxide sites with variable oxidation states. T his complexity makes it inherently difficult to un derstand it s ac tivity an d se lectivity in catalytic reactions. In this work, we used multilayer cluster models of the main catalytic active site of M1. We explored surface dynamics and surface oxidation by O_2, oxygen vacancy formation on metal sites and the chemo- and regioselectivity of propane activation on the surface. Our investigation shows that linear scaling relationships to estimate free energy activation barriers using a simple descriptor such as the hydrogen binding energy hold true for M1. We have established a mechanistic model of the full catalytic cycle for a radical-like pathway for propane oxidation to propene on M1.

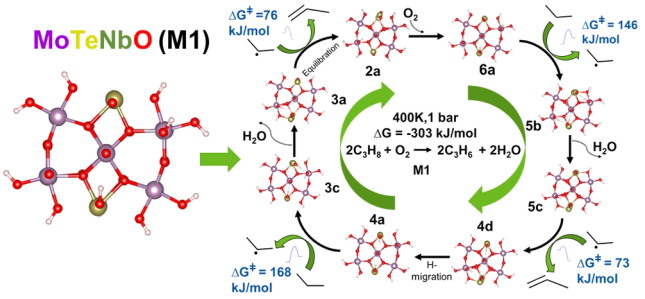

INTRODUCTION

The activation of C−H bonds constitutes the first step for the functionalization of hydrocarbons toward higher value chemicals. Usually, this activation is achieved through cofeeding of oxygen, which often also leads to oxygenated products, which play an important role as a feedstock for a large number of chemicals. However, these oxidation processes need to be highly selective, as one would otherwise obtain undesired side products and here in particular CO_2. Devising heterogeneous catalysts that are highly selective is thus a crucial prerequisite for implementation in the chemical industry.[1,2] One example is given by the industrial conversion of propane to acrylic acid over the M1/M2 phase of a MoVTeNbO mixed-metal oxide (MMO) catalyst.[3−17] This catalyst has shown 61% selectivity for the conversion of propane to acrylic acid[18−21] at 380 °C. Selective oxidative dehydrogenation of both ethane and propane can also be achieved with this catalyst.[22−24]

This MMO catalyst contains four metals and has a rather complex structure. It is believed that the (001) facet of bulk M1 is responsible for the observed catalytic activity.[25−27] This facet contains several structural motifs such as a 5-membered ring of Mo surrounding Nb and 7- and 6-membered rings of Mo/V surrounding Te.[28,29] There is also additional complexity from the variation of the oxidation states of metal sites such as Mo^{6+}/Mo^{5+}, Mo^{6+}/V^{+5}, Mo^{5+}/V^{+4}, Te^{4+}, Te^{2+}, and Nb^{5+}.

Naumann d'Alnoncourt et al.[20] have observed that the surface of M1 changes dynamically and reversibly with the change of feed composition. The presence of steam in the feed changes the oxidation states of surface metals, and it also correlates with the selectivity toward acrylic acid. Steam causes enrichment of V and Te on the surface at the expense of Mo. They also observed that high O_2 concentration in the feed keeps the catalyst in a high oxidation state. They measured the activation energy of propane in a dry feed to be 80−95 kJ/mol, which is reduced to 55−75 kJ/mol in a wet feed. Kube et al.[22] reported the activation of propane to propene on M1 starting at low temperature (120 °C); hence, first CH activation, which is the rate-determining step, is not the only issue for M1 for producing valuable chemicals. They reported that quasi-simultaneous H-abstraction on neighboring M═O sites based on kinetic isotope effects should be a more favorable pathway compared to first CH-activation at the middle carbon of propane and radical like pathway toward propene. They have observed production of several intermediate gas species and overoxidation to CO/CO_2 with increasing reaction temperature (100−400 °C) and proposed a possible reaction network over the surface as an initial picture.

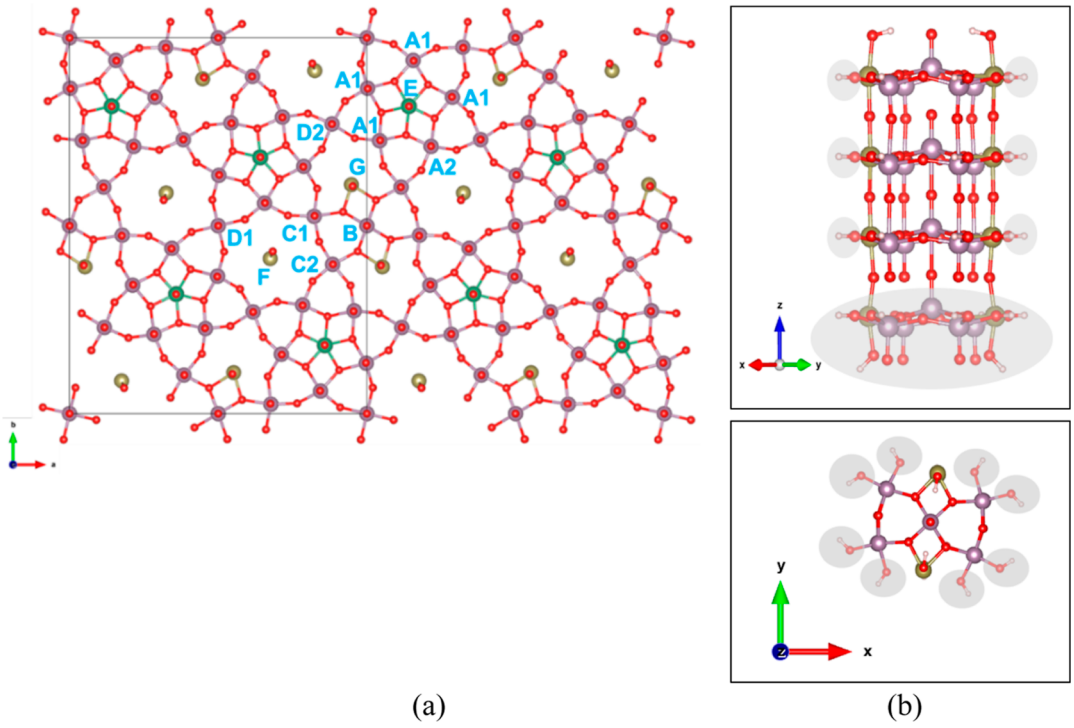

Figure 1. (a) Top view of the (001) facet of the unit cell of MMO-M1 (MoVTeNbO) (ICSD-55097). Mo/V atoms are shown in violet, Nb in green, Te in yellow, and oxygen in red. A1, A2, B, C1, C2, D1, and D2 are different unique Mo/V sites; E is for Nb and F; and G are two different Te sites present. (b) Side and top views of a 4-layer cluster model of the catalytically most active site consisting of C1, C2, B, and G sites (highlighted by a light lavender rectangle in a) with broken bond termination by OH groups (frozen atoms in the calculations are marked by greyed circles).

Nevertheless, the reaction mechanism from propane to acrylic acid is quite complex and thus still not entirely understood.[10] Owing to the importance of the process, the selective propane oxidation over M1/M2 has also been subject to several theoretical studies. It has been proposed that C−H abstraction and successive C−O bond formation at allylic positions of different gas-phase intermediates are the key steps in the above-mentioned pathways which determine not only activity but also selectivity.[30] Liu et al. used the concept of H atom addition energy, steric effects, and the effects of spin multiplicity to understand different active sites on the surface of M1.[30,31] They performed a comparative study of the activation of propane mainly at the porous site of M1 and on the (001) surface of a V_2O_5 catalyst. Due to the large unit cell and the complexity in terms of Mo/V substitution and related oxidation states, simple models of M1 have been invoked. Cheng and Goddard[32,33] investigated the reduction-coupled oxo activation mechanism for propane to propene on Te−V−Te clusters where a propyl radical binds to the central V═O after the first C−H activation, then transfers the second proton to a Te═O site, and finally dissociates from the surface to form propene. While this serves as a good starting point to understand how M1 catalysts facilitate the reaction, these models ignore the role of neighboring M-Oxo sites in activating the CH bond and their effect on the full reaction mechanism. Studies of ODH on M1 by Li et al.[34] show correlations between adsorption energies of hydrogen atoms on the surface to the reaction energy and also to the activation barrier of the C−H activation of the alkanes. Based on their findings, they proposed a vertical migration of electrons from the top to the middle layer during the reaction.

An extensive study invoking a full catalytic cycle employing the entire active site is missing to date. This is the aim of the current study, where we show that due to the multireference characteristics of M1, it is challenging to produce accurate energies with density functional theory (DFT), necessitating the use of hybrid DFT. We also employ larger cluster models of the complete active site, hence capturing the entire complexity of M1 in terms of its electronic structure.

Our focus is on a Mo-only model as a starting point such that a simple reaction scheme covering the entire catalytic cycle can be established. More realistic catalysts typically incorporate one or more V atoms;[29] the location and influence on the catalytic activity are not being fully understood to date. As this will add much more complexity, depending on the location of the V atoms, we used a Mo-only model here as a starting point; future work will explore the influence of V substitution.

We use this Mo-only model to investigate the oxygen activation, surface dynamics, and oxidation of propane to propene as the first important reaction step of propane functionalization. Based on extensive DFT calculations, we are able to suggest for the first time the reaction energetics of a full catalytic cycle that also includes the activation of O_2 and the production of water.

COMPUTATIONAL DETAILS

All DFT calculations for cluster models were performed using the quantum chemistry molecular code TURBOMOLE.[35] All geometry optimizations have been performed within the generalized gradient approximation (GGA) using the PBE functional,[36,37] with split valence basis sets (def2-SVP).[38] Single-point energy calculations have been performed using the

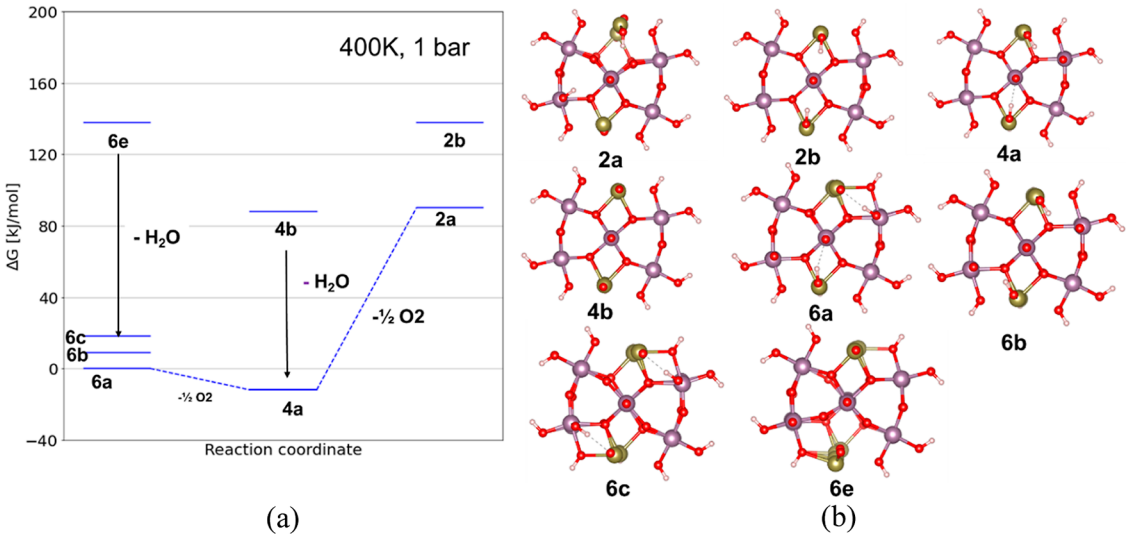

Figure 2. (a) ΔG profile of consecutive reduction of the cluster surface at 400 K and 1 bar pressure of oxygen and water. For each SOX category, the Gibbs free energy levels of different OH distributions and different amounts of chemisorbed H_2O (**4b** and **6e**) are shown. (b) Top view of the active site structures. Colors are the same as in Figure 1.

meta hybrid-DFT functional M06[39−41] (see the Supporting Information for detailed analysis and benchmarking in Figures S7−S10), triple-ζ valence basis sets with two sets of polarization functions (def2-TZVPP),[38] and higher convergence criteria of 10^{-7} with the optimized geometry for all data presented in this work (see Table ST3 in the Supporting Information for all PBE-D3 and M06-D3 energies). An extensive benchmark from Goerigk and Grimme[42] showed that adding D3 dispersion correction in general improved the description of noncovalent interaction as well as reaction energies. Therefore, the Grimme et al. D3 dispersion correction[43] was applied for all our calculations (hence PBE-D3 and M06-D3).[42,44] Open shell calculations have been performed within the unrestricted Kohn−Sham framework.[45] We have performed the spin states of singlet, triplet, and quintet for even number of electrons or doublet, quartets, and sextets for uneven number of electrons and selected the spin state with the lowest energy to obtain the final single-point electronic energy. Our initial investigation shows that only the choice of these three initial spin states is sufficient to obtain the ground-state energy because energy becomes exponentially higher with further high spin states (plots are provided in Supporting Information Figure S5). Initial analysis of bulk model has been performed using the Vienna Ab Initio Simulation Package software package (VASP).[46−48]

ACTIVE SITE MODELING

The orthorhombic unit cell of M1 - MoVTeNbO (ICSD-55097) contains 168 atoms with lattice parameters a = 20.385 Å, b = 25.935 Å, and c = 4.800 Å after bulk optimization. Figure 1a shows the different surface motifs of 7-membered rings of Mo/V surrounding Te═O (F site), 5-membered rings of Mo surrounding Nb═O (E site), and a 4-membered motif surrounding a 2TeO (G site) and 1 Mo/V═O (B site) structure. Two Nb ring sites are connected via a Mo/V bridge (C and D sites).

Lattice oxygens connect the metal sites to each other within the layers of the catalyst, and the connectivity to oxygen atoms in the neighboring layer above or below determines the oxidation states of the metal atoms. To understand the oxidation states of different metal sites, we analyzed metal−oxygen bond distances, coordination number, charge, and spin analysis which resulted in a distribution of oxidation states according to Figure S1 in the Supporting Information. According to these findings, Mo at A1 and A2 sites surrounding Nb have the oxidation states 6+ and 5+, respectively. Every other Mo atom (at B, C, and D sites) is in the 5+ oxidation state. Te at sites F and G is 2+ and 4+, respectively. This is also consistent with the Bader charge distribution and unpaired spin analysis from periodically optimized bulk structure data, Figure S2 in the Supporting Information, in which we find significant unpaired electron density at all 2+, 4+, and 5+ sites and almost no spin at Mo (6+) sites. Govindasamy et al.[49] has performed the first theoretical study to investigate the cluster models of the active site of the MoVTeNbO MMO catalyst. According to them, the function of the pentagonal Nb site is to stabilize the structure and provide active site isolation for catalytic reactions.

The active site[28,29,50] is chosen such that it consists of C1, C2, B, and G metal sites (rectangular light green zone of Figure 1a). All broken metal−oxygen bonds at the edge of the cluster have been terminated by hydrogen atoms with the standard OH distances of 0.97 Å[51] and with an orientation in the direction of the replaced metal centers. The in-plane terminating OH groups have been kept fixed during all structure optimizations (circular grayed part of Figure 1b).

We performed systematic investigations of oxidation energies by addition of oxygen atoms on the surface, Bader charge analysis, and spin density on Mo atoms with increasing number of layers (Figure S6 in the Supporting Information) These properties converged with a 4-layer model, which we chose as our working model of the active site of the M1 catalyst. All atoms in the lowest layer were kept frozen during optimization (greyed parts in Figure 1b).

RESULTS AND DISCUSSION

Oxidation of the Active Site Using O_2. We started by investigating the surface composition under the reaction conditions. The Mo_5Te_2 cluster has one central Mo (denoted M_c) and 4 symmetry equivalent side Mo (denoted as M_s, see

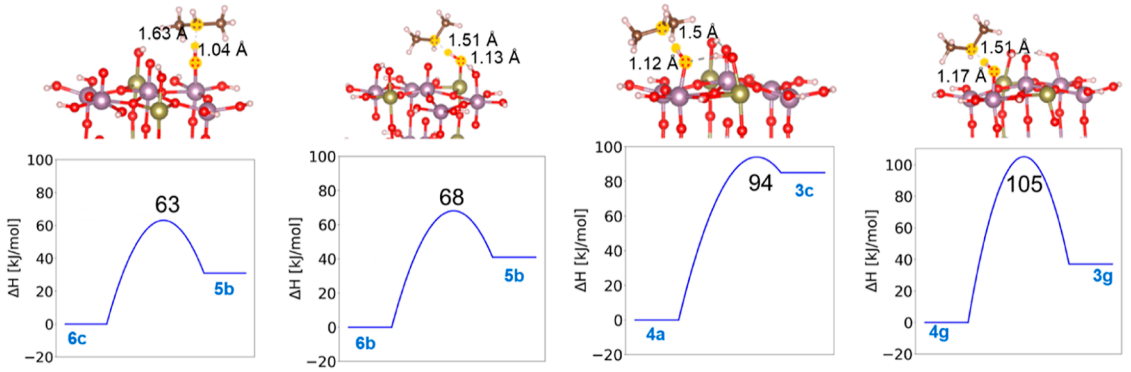

Figure 3. Activation barrier for propane (M06-D3/def2-TZVPP) at the central carbon atom on four different surface configurations **6c** → **5b** (63 kJ/mol), **6b** → **5b** (68 kJ/mol), **4a** → **3c** (94 kJ/mol), and **4g** → **3g** (105 kJ/mol) from left to right. TS structures with C−H−O bond distances are shown on top.

Figure 1b). Two Te atoms are attached to the oxygen atoms bridging M_c and M_s. We generally find that oxygen (and hydroxyl) binds on these in energetic order M_c, Te, and M_s, with M_c having the strongest Mo−O bond. We calculated the surface coverage of all possible O and OH, and the free energy of this is shown in Figure 2a. The surface oxidation state (SOX) for a certain surface configuration is calculated using the following formula

$$\mathrm{SOX} = 2^{*}\ \eta_{\mathrm{O}} + \eta_{\mathrm{OH}}$$

where η_O = no. of oxygen on M_s or Te and η_{OH} = no. of OH on the surface.

In the following, we label the surface configuration with the SOX as the first digit, followed by a letter denoting its energetic ranking in alphabetical order (Figure 2b). For example, surface **4b** has a SOX of 4 and is the second most stable surface in that SOX category. We investigated the extent to which the hydrogen atoms at the hydroxyl groups are mobile and found that diffusion barriers (hydrogen migration from one O to the nearest neighbor O) are relatively small, typically being less than 20 kJ/mol. Importantly, hydrogen diffusion to a hydroxyl group (OH*) producing a water molecule is similarly fast (TS structures are shown in Figure S15a,b in the Supporting Information). We hence conclude that the catalyst surface is always in its thermodynamic equilibrium with respect to the O-bound to H atom distribution under reaction conditions as well as with the dissociation of water via H-migration (on a O atom) to a neighboring OH site. All top view of the surfaces with their id and their energies are presented in Tables ST2 and ST3 of the Supporting Information pdf file. The xyz files are provided in Supporting Information zip folder, and here, we focus on the most relevant one from the energetic point of view. The blue dotted line in Figure 2a shows the most favorable surface oxidation/reduction path connecting the **2a**, **4a**, and **6a** configurations, whereas other configurations such as **6e**, **6b**, **6c**, **4b**, and **2b** will either isomerize via H-migration or desorb and reabsorb water to achieve the most stable surface states on the blue line.

Given the thermodynamics of surface oxidation, we assume the successive catalytic oxidation of two propane molecules with molecular O_2 cycles between a SOX of 2 and 6, making it a 4-electron process. Even though **4a** is the most stable surface (see Figure 2a), our aim in this study is to show the entire catalytic mechanism. We therefore start our catalytic cycle at SOX **6a**. However, as the configurations with higher free energy could also be considerably populated under reaction conditions, we considered the activation of propane on these structural models as well. As this gives rise to a large number of transition states, we aimed to establish scaling relations as described below to simplify this task.

Linear Scaling Relation for CH Activation of Propane and Propyl Molecules. Earlier theoretical studies established that the transition-state energy of C−H bond activation scales linearly with the binding energies of a hydrogen atom on the respective surface oxygen, denoted as E_H, with a slope of 0.75.[52] This observation has been made for radical-like transition states of hydrocarbon activation over a range of materials including oxides and been investigated mostly for the case of methane, but ethane activation has been found to obey a similar universal scaling relation. Busch et al.[44] has benchmarked the linear free energy scaling relationships among binding energies of *−OH, *═O, and *−OOH (intermediate species for oxygen evolution reaction (OER)) on different solid and molecular catalysts with several DFT functionals against GMC-QDPT2, a multiconfigurational method based on relativistic quasi-degenerate perturbation theory.[53,54] According to them, hybrid functionals with a lower amount of exact exchange have minimum error and typically underbind the intermediates. Among them, M06 and PBE0 are the best performing hybrid functionals, besides less expensive M06-L, to describe linear scaling for the OER. We have calculated various transition states, dealing with the activation of propane (primary and secondary carbon atoms) and the H-abstraction from propyl. Optimized transition-state geometries and related reaction barriers for the activation of the secondary carbon are shown in Figure 3. As can be seen, barrier heights are on the order of 60−100 kJ/mol for the structures investigated. Note that the activation of the primary carbon always has a somewhat higher activation barrier, as one would expect (data given in the Supporting Information in Table ST4). Recent work from Yu et al.[50] also established a linear relationship between the C−H activation energy and the hydrogen binding energy (ΔE_H). They, however, observed a much wider range of activation energies (from 80 to 200 kJ/mol) and a scaling with a slope of 1 at the GGA level of theory (see also Figure S11a in the Supporting Information). Contrarily, other works calculated a slope of 0.6 for the same reaction albeit on V_2O_5 and V_2O_5/TiO_2 (see Figure S11b in the Supporting Information) for the catalyst.[34,55] In this work, we found an analogous scaling relation, but having a

slope of 0.75 along the lines of what has been reported for methane, ethane, and methanol activation over a wide range of catalysts.[52] We therefore employ the scaling with a slope of 0.75 identified herein to estimate the reaction barriers for all reaction steps.

We also find that the difference in intercept is the difference in molecular C−H bond energies of 18.6 kJ/mol (Figure 4), and the line fits the calculated date points very well (data points in magenta in Figure 4). All the 4 transition states for propane activation are shown in Figure 3.

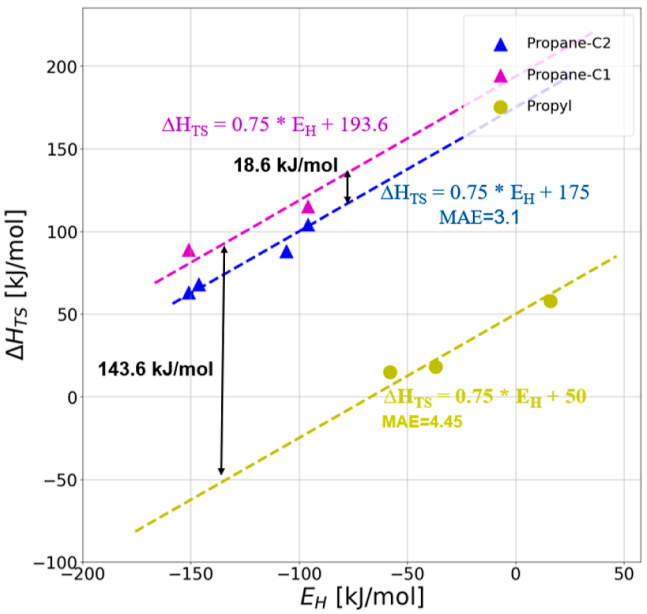

Figure 4. Linear scaling lines for H abstraction at C1 of propane (purple line), for H abstraction at C2 (blue line), and for H abstraction at C1 of propyl (yellow line) on the M1 catalyst between E_H and H_{TS} for 5 Mo on the surface. The enthalpy differences between different lines are shown with black arrows.

The first C−H bond activation produces a propyl radical. We investigated the second C−H activation of the propyl radical and generally found much lower barriers, again in line with the much lower C−H bond strength of the propyl radical (being 180 kJ/mol). The difference in C−H bond strength between the activating terminal C−H bond in gas-phase propane and propyl is 270 kJ/mol (see Table ST4 in the Supporting Information). We found the yellow line which is 144 kJ/mol lower than the magenta line, fits the propyl data points well (Figure 4). This smaller activation barrier can be explained by the stabilization of the propyl radical on the surface M═O site and activating the C−H bond at the terminal site, which makes the activation barrier higher compared to the gas-phase C−H bond strength difference. We thus conclude that we can use the hydrogen binding energy (ΔE_H) as a descriptor for C−H activation over the investigated catalyst models. Calculations of entropy contributions at the transition states reveal that these are roughly similar among the structures investigated here (see Table ST1 in the Supporting Information for details), and we hence assume them to be constant for the same C−H activation processes.

Using the scaling relations shown in Figure 4, we calculated the full catalytic cycle of the conversion of 2 propane molecules and molecular oxygen. Figure 5 shows the resulting free energy diagram at a temperature of 400 K and a pressure of 1 bar. The enthalpy of activation barriers is estimated from the linear scaling lines. We have added a constant shift of 73 kJ/mol for the entropic contribution to the enthalpy of the activation barrier to obtain the Gibbs free energy at 400 K. This value is obtained by averaging all of the calculated entropies of the transition states (Table ST1 in the Supporting Information).

Full Catalytic Cycle. The starting point is the fully oxidized surface (SOX = 6), which reacts with one propane to create propene and a surface with SOX = 4. After conversion of another propane to propene, the resulting surface (SOX = 2) is reoxidized using molecular oxygen, thus establishing a full catalytic cycle (Figure 5). Importantly, using the scaling

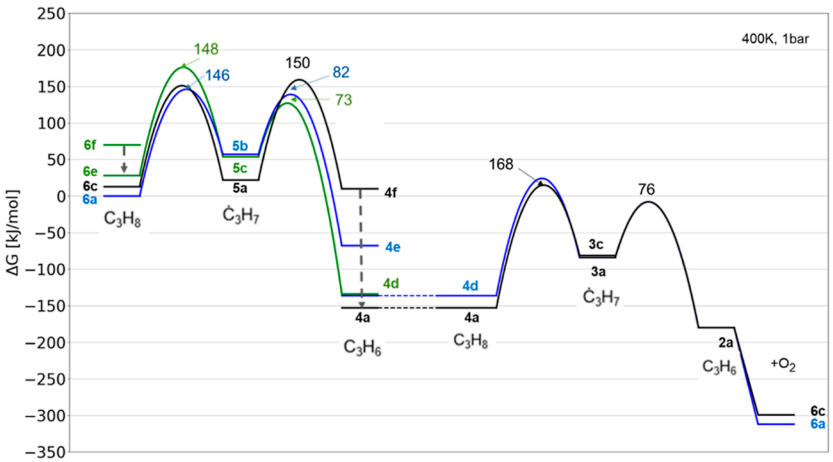

Figure 5. Free energy diagram for the full catalytic cycle of oxidation of 2 propane molecules to 2 propene and 2 water molecules at 400 K and 1 bar. All energies are given relative to ideal gas-phase propane, propyl, or propene molecules and catalyst. **6a** is the initial structure and has the lowest propane activation barrier of 146 kJ/mol (blue) to **5b**. **5b** will desorb water to **5d** which has the lowest activation barrier of 73 kJ/mol for propyl to propene (green line) to **4d**. **4d** will be stabilized to **4a** via H-migration. A high second propane activation barrier of 168 kJ/mol is observed at **4a** to **3c**, followed by water desorption to **3a** and propyl activation to form the second propene molecule on **2a**. **2a** will be oxidized by O_2 to form **6a** to complete the catalytic cycle. Activation barriers are estimated from the linear scaling relations in Figure 4. The black dotted arrows correspond to water desorption.

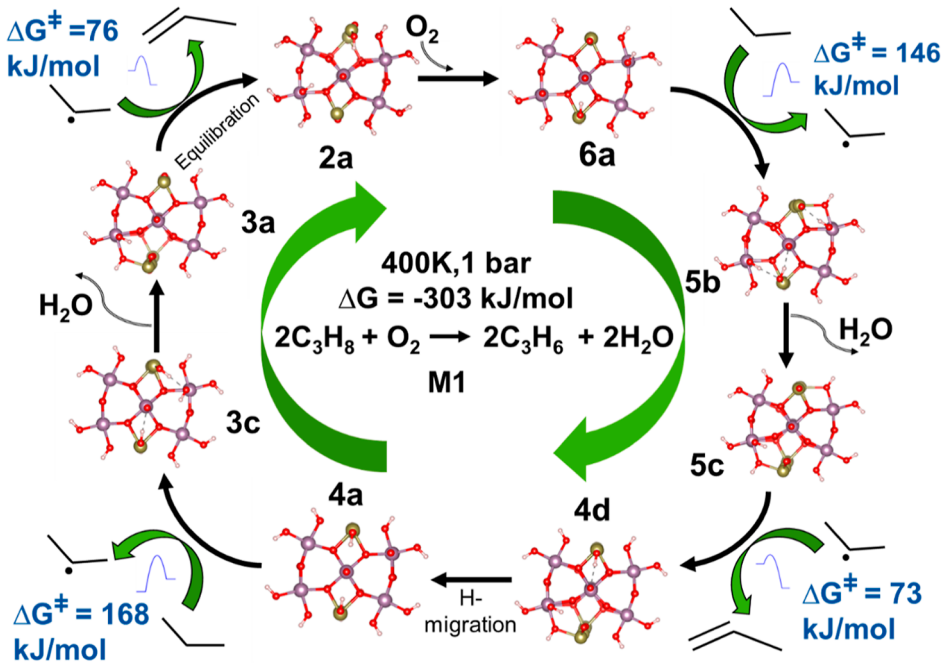

Figure 6. Final minimum energy pathway summarized from Figure 5 of the full catalytic cycle of oxidation of 2 propane molecules to form 2 propene and 2 water molecules. The top view of the surface states, their id, and 4 activation barriers are shown here.

relations established in Figure 4, we connected various energetically close surfaces, hence obtaining a comprehensive reaction mechanism. As discussed above, we assume that, due to low barriers of hydrogen diffusion, all surfaces are in thermodynamic equilibrium, including the adsorption and desorption of water. The obtained final minimum free energy pathway with activation barriers is shown in Figure 6.

We have explored all possible energetic pathways for the mechanisms shown in Parts S12–S14 in the Supporting Information, whereas Figure 5 shows only the minimum energy pathways for C–H activation of the central carbon of propane, as this is always lower in energy than for the terminal carbon. The black and blue lines are the pathways where water desorption from **4f**/**4e** to **4a** creates an O vacancy at a Mo site, whereas the green line starts from dissociative adsorption of an O_2 molecule in neighboring M_c sites (**6f**), followed by a water desorption to **6e**. The first reaction free energy barrier is 146 kJ/mol (TS1, blue line). After that, the propyl radical reacts further with a barrier of about 73 kJ/mol (TS2, green line) when referenced to the preceding propyl radical. This leads to surfaces with the SOX = 4. Equilibration (through water desorption) yields structure **4a** as being most stable under the chosen reaction conditions. This process is about 150 kJ/mol exothermic. The activation of a second propane over **4a** has a barrier (TS3) of 168 kJ/mol, followed by conversion of the propyl radical with a barrier of 76 kJ/mol when the preceding propyl radical. This process is only exothermic by 20 kJ/mol after equilibration to the most stable surface (again accompanied by water desorption). Importantly, the surface of **2a** has only M_s (**2a** in Figure 2b), such that there is space for the splitting of molecular O_2 along the Mo–O–Mo axis. As hydrogen migration and water adsorption/desorption processes are rather fast, later the oxygen atom on the nearby Mo atom will migrate to the Te atom for thermodynamics reason (see Figure S19 in the Supporting Information for additional information). This process is calculated to be exothermic by 150 kJ/mol. This last step concludes the full catalytic cycle, again establishing surface **6a**.

The highest barrier in the entire reaction mechanism is thus the activation of the second propane, which is 168 kJ/mol. Using the energy span model,[56] this will yield a rate of about 1.58×10^{-8} s^{-1} at 150 °C, keeping in mind that the typical error from DFT calculations is ±2 orders of magnitude at this temperature;[77] however, our model does not contain any V atoms in Mo sites. How these influence the reaction barriers is outside the scope of the current contribution and will be dealt with in a subsequent work.[57−76]

CONCLUSIONS

In this work, we have established a full catalytic cycle for the selective oxidation of propane to propene on the M1 phase of the MoTeNbO catalyst. This was aided through establishing linear scaling relations using a simple descriptor, such as the hydrogen binding energy. Importantly, we found that the intercept of the scaling is dependent on the C–H bond strength, opening avenues to predict scaling lines without any transition-state calculations. Our investigation shows that the Mo-only catalyst will be comparatively inactive due to the high C–H activation barrier for the second propane molecule. How this will change upon substitution with V atoms remains to be seen but could explain the superior performance of V-substituted catalysts. We should also keep in mind, however, that we focused on the first oxidation step only, i.e., propane to propene. A deeper mechanistic understanding of the reactivity of propyl radicals on the surface, the oxidation of formed propene, and further CH activation processes ultimately leading to acrylic acid are required in order to understand the limiting factors of M1 catalysts.

AUTHOR INFORMATION

Corresponding Authors

Karnajit Sen − *BASF SE, RGQ/SQ - B001, 67056 Ludwigshafen am Rhein, Germany;* orcid.org/0000-0002-4163-3969; Email: karnajitsen@gmail.com

Felix Studt − *Institute of Catalysis Research and Technology (IKFT), Karlsruhe Institute of Technology (KIT), 76344 Eggenstein-Leopoldshafen, Germany;* orcid.org/0000-0001-6841-4232; Email: felix.studt@kit.edu

Authors

Ansgar Schäfer − *BASF SE, RGQ/SQ - B001, 67056 Ludwigshafen am Rhein, Germany*

Frank Rosowski − *BasCat, UniCat BASF JointLab, 10623 Berlin, Germany; BASF SE, Catalysis Research, 67065 Ludwigshafen, Germany*

Dmitry I. Sharapa − *Institute of Catalysis Research and Technology (IKFT), Karlsruhe Institute of Technology (KIT), 76344 Eggenstein-Leopoldshafen, Germany;* orcid.org/0000-0001-9510-9081

Funding

T his project is funded by the catalysis research division of BASF SE. All computations are performed using onsite supercomputer Quriosity at BASF SE, Ludwigshafen, Germany.

Notes

The authors declare no competing financial interest.

ACKNOWLEDGMENTS

A special thanks to Dr. Annette Trunschke from FHI Berlin for valuable ideas and discussions and BASF SE to provide computational resources of their HPC machine for quantum chemical calculation.

REFERENCES

(1) Brazdil, J. F. Strategies for the Selective Catalytic Oxidation of Alkanes. *Top. Catal.* **2006**, *38* (4), 289−294.

(2) Li, X.; Teschner, D.; Streibel, V.; Lunkenbein, T.; Masliuk, L.; Fu, T.; Wang, Y.; Jones, T.; Seitz, F.; Girgsdies, F.; et al. How to Control Selectivity in Alkane Oxidation? *Chem. Sci.* **2019**, *10* (8), 2429−2443.

(3) Védrine, J. C. Heterogeneous Partial (Amm)Oxidation and Oxidative Dehydrogenation Catalysis on Mixed Metal Oxides. *Catalysts* **2016**, *6* (2), 22.

(4) Faramawy, S.; Zaki, T.; Sakr, A. A.-E. Natural Gas Origin, Composition, and Processing: A Review. *J. Nat. Gas Sci. Eng.* **2016**, *34*, 34−54.

(5) Wachs, I. E.; Routray, K. Catalysis Science of Bulk Mixed Oxides. *ACS Catal.* **2012**, *2* (6), 1235−1246.

(6) Sprenger, P.; Kleist, W.; Grunwaldt, J.-D. Recent Advances in Selective Propylene Oxidation over Bismuth Molybdate Based Catalysts: Synthetic, Spectroscopic, and Theoretical Approaches. *ACS Catal.* **2017**, *7* (9), 5628−5642.

(7) Deshlahra, P.; Carr, R. T.; Chai, S.-H.; Iglesia, E. Mechanistic Details and Reactivity Descriptors in Oxidation and Acid Catalysis of Methanol. *ACS Catal.* **2015**, *5* (2), 666−682.

(8) Shiju, N. R.; Liang, X.; Weimer, A. W.; Liang, C.; Dai, S.; Guliants, V. V. The Role of Surface Basal Planes of Layered Mixed Metal Oxides in Selective Transformation of Lower Alkanes: Propane Ammoxidation over Surface *Ab* Planes of Mo−V−Te−Nb−O M1 Phase. *J. Am. Chem. Soc.* **2008**, *130* (18), 5850−5851.

(9) Andrushkevich, T. V.; Ovchinnikova, E. V. The Role of Water in Selective Heterogeneous Catalytic Oxidation of Hydrocarbons. *Mol. Catal.* **2020**, *484*, 110734.

(10) Schlögl, R. Active Sites for Propane Oxidation: Some Generic Considerations. *Top. Catal.* **2011**, *54* (10−12), 627−638.

(11) Grasselli, R. K.; Buttrey, D. J.; Burrington, J. D.; Andersson, A.; Holmberg, J.; Ueda, W.; Kubo, J.; Lugmair, C. G.; Volpe, A. F. Active Centers, Catalytic Behavior, Symbiosis and Redox Properties of MoV(Nb,Ta)TeO Ammoxidation Catalysts. *Top. Catal.* **2006**, *38* (1−3), 7−16.

(12) Schlögl, R. Selective Oxidation: From a Still Immature Technology to the Roots of Catalysis Science. *Top. Catal.* **2016**, *59* (17−18), 1461−1476.

(13) Hävecker, M.; Wrabetz, S.; Kröhnert, J.; Csepei, L.-I.; Naumann d'Alnoncourt, R.; Kolen'ko, Y. V.; Girgsdies, F.; Schlögl, R.; Trunschke, A. Surface Chemistry of Phase-Pure M1MoVTeNb Oxide during Operation in Selective Oxidation of Propane to Acrylic Acid. *J. Catal.* **2012**, *285* (1), 48−60.

(14) Sanfiz, A. C.; Hansen, T. W.; Teschner, D.; Schnörch, P.; Girgsdies, F.; Trunschke, A.; Schlögl, R.; Looi, M. H.; Hamid, S. B. A. Dynamics of the MoVTeNb Oxide M1 Phase in Propane Oxidation. *J. Phys. Chem. C* **2010**, *114* (4), 1912−1921.

(15) Wernbacher, A. M.; Kube, P.; Hävecker, M.; Schlögl, R.; Trunschke, A. Electronic and Dielectric Properties of MoV-Oxide (M1 Phase) under Alkane Oxidation Conditions. *J. Phys. Chem. C* **2019**, *123* (21), 13269−13282.

(16) Fan, Y.; Li, S.; Liu, Y.; Wang, Y.; Wang, Y.; Chen, Y.; Yu, S. High-Pressure Hydrothermal Synthesis of MoVTeNbOx with High Surface V5+ Abundance for Oxidative Conversion of Propane to Acrylic Acid. *J. Supercrit. Fluids* **2022**, *181*, 105469.

(17) Shorayeva, K. A.; Massalimova, B. K.; Bespalko, Y. N.; Kovalev, E. P.; Ishchenko, A. V.; Sadykov, V. A. Synthesis, Properties, and Activity of MoVTeNbO Catalysts Modified by Zirconia-Pillared Clays in Oxidative Dehydrogenation of Ethane. *Open Chem.* **2021**, *19* (1), 492−502.

(18) Duprez, D.; Cavani, F. *Handbook of Advanced Methods and Processes in Oxidation Catalysis: From Laboratory to Industry*; Imperial College Press, 2014; ..

(19) Trunschke, A.; Noack, J.; Trojanov, S.; Girgsdies, F.; Lunkenbein, T.; Pfeifer, V.; Hävecker, M.; Kube, P.; Sprung, C.; Rosowski, F.; et al. The Impact of the Bulk Structure on Surface Dynamics of Complex Mo−V-Based Oxide Catalysts. *ACS Catal.* **2017**, *7* (4), 3061−3071.

(20) Naumann d'Alnoncourt, R.; Csepei, L.-I.; Hävecker, M.; Girgsdies, F.; Schuster, M. E.; Schlögl, R.; Trunschke, A. The Reaction Network in Propane Oxidation over Phase-Pure MoVTeNb M1 Oxide Catalysts. *J. Catal.* **2014**, *311*, 369−385.

(21) Amakawa, K.; Kolen'ko, Y. V.; Villa, A.; Schuster, M. E.; Csepei, L.-I.; Weinberg, G.; Wrabetz, S.; Naumann d'Alnoncourt, R.; Girgsdies, F.; Prati, L.; et al. Multifunctionality of Crystalline MoV(TeNb) M1 Oxide Catalysts in Selective Oxidation of Propane and Benzyl Alcohol. *ACS Catal.* **2013**, *3* (6), 1103−1113.

(22) Kube, P.; Frank, B.; Schlögl, R.; Trunschke, A. Isotope Studies in Oxidation of Propane over Vanadium Oxide. *ChemCatChem* **2017**, *9* (18), 3446−3455.
(23) Donaubauer, P. J.; Melzer, D. M.; Wanninger, K.; Mestl, G.; Sanchez-Sanchez, M.; Lercher, J. A.; Hinrichsen, O. Intrinsic Kinetic Model for Oxidative Dehydrogenation of Ethane over MoVTeNb Mixed Metal Oxides: A Mechanistic Approach. *Chem. Eng. J.* **2020**, *383*, 123195.
(24) Annamalai, L.; Liu, Y.; Ezenwa, S.; Dang, Y.; Suib, S. L.; Deshlahra, P. Influence of Tight Confinement on Selective Oxidative Dehydrogenation of Ethane on MoVTeNb Mixed Oxides. *ACS Catal.* **2018**, *8* (8), 7051−7067.
(25) Celaya Sanfiz, A.; Hansen, T. W.; Sakthivel, A.; Trunschke, A.; Schlogl, R.; Knoester, A.; Brongersma, H. H.; Looi, M. H.; Hamid, S. B. A. How Important Is the (001) Plane of M1 for Selective Oxidation of Propane to Acrylic Acid? *J. Catal.* **2008**, *258* (1), 35−43.
(26) DeSanto, P.; Buttrey, D. J.; Grasselli, R. K.; Lugmair, C. G.; Volpe, A. F.; Toby, B. H.; Vogt, T. Structural Aspects of the M1 and M2 Phases in MoVNbTeO Propane Ammoxidation Catalysts. *Z. Kristallogr. Cryst. Mater.* **2004**, *219* (3), 152−165.
(27) Li, X.; Buttrey, D. J.; Blom, D. A.; Vogt, T. Improvement of the Structural Model for the M1 Phase Mo−V−Nb−Te−O Propane (Amm)Oxidation Catalyst. *Top. Catal.* **2011**, *54* (10−12), 614−626.
(28) Masliuk, L.; Heggen, M.; Noack, J.; Girgsdies, F.; Trunschke, A.; Hermann, K. E.; Willinger, M. G.; Schlögl, R.; Lunkenbein, T. Structural Complexity in Heterogeneous Catalysis: Cataloging Local Nanostructures. *J. Phys. Chem. C* **2017**, *121* (43), 24093−24103.
(29) Grasselli, R. K.; Lugmair, C. G.; Volpe, A. F. Towards an Understanding of the Reaction Pathways in Propane Ammoxidation Based on the Distribution of Elements at the Active Centers of the M1 Phase of the MoV(Nb,Ta)TeO System. *Top. Catal.* **2011**, *54* (10−12), 595−604.
(30) Liu, Y.; Twombly, A.; Dang, Y.; Mirich, A.; Suib, S. L.; Deshlahra, P. Roles of Enhancement of C−H Activation and Diminution of C−O Formation Within M1-Phase Pores in Propane Selective Oxidation. *ChemCatChem* **2021**, *13* (3), 882−899.
(31) Deshlahra, P.; Iglesia, E. Reactivity and Selectivity Descriptors for the Activation of C−H Bonds in Hydrocarbons and Oxygenates on Metal Oxides. *J. Phys. Chem. C* **2016**, *120* (30), 16741−16760.
(32) Cheng, M.-J.; Goddard, W. A. The Mechanism of Alkane Selective Oxidation by the M1 Phase of Mo−V−Nb−Te Mixed Metal Oxides: Suggestions for Improved Catalysts. *Top. Catal.* **2016**, *59* (17−18), 1506−1517.
(33) Cheng, M.-J.; Goddard, W. A. I. In Silico Design of Highly Selective Mo-V-Te-Nb-O Mixed Metal Oxide Catalysts for Ammoxidation and Oxidative Dehydrogenation of Propane and Ethane. *J. Am. Chem. Soc.* **2015**, *137* (41), 13224−13227.
(34) Li, W.-Q.; Fjermestad, T.; Genest, A.; Rösch, N. Reactivity Trends of the $MoVO_x$ Mixed Metal Oxide Catalyst from Density Functional Modeling. *Catal. Sci. Technol.* **2019**, *9* (7), 1559−1569.
(35) Balasubramani, S. G.; Chen, G. P.; Coriani, S.; Diedenhofen, M.; Frank, M. S.; Franzke, Y. J.; Furche, F.; Grotjahn, R.; Harding, M. E.; Hättig, C.; Hellweg, A.; Helmich-Paris, B.; Holzer, C.; Huniar, U.; Kaupp, M.; Marefat Khah, A.; Karbalaei Khani, S.; Müller, T.; Mack, F.; Nguyen, B. D.; Parker, S. M.; Perlt, E.; Rappoport, D.; Reiter, K.; Roy, S.; Rückert, M.; Schmitz, G.; Sierka, M.; Tapavicza, E.; Tew, D. P.; van Wüllen, C.; Voora, V. K.; Weigend, F.; Wodynski, A.; Yu, J. M. Turbomole: Modular program suite for ab initio quantum-chemical and condensed-matter simulations. *J. Chem. Phys.* **2000**, *152*, 184107.
(36) Ernzerhof, M.; Scuseria, G. E. Assessment of the Perdew−Burke−Ernzerhof Exchange-Correlation Functional. *J. Chem. Phys.* **1999**, *110* (11), 5029−5036.
(37) Perdew, J. P.; Burke, K.; Ernzerhof, M. Generalized Gradient Approximation Made Simple. *Phys. Rev. Lett.* **1996**, *77* (18), 3865−3868.
(38) Weigend, F.; Ahlrichs, R. Balanced Basis Sets of Split Valence, Triple Zeta Valence and Quadruple Zeta Valence Quality for H to Rn: Design and Assessment of Accuracy. *Phys. Chem. Chem. Phys.* **2005**, *7* (18), 3297.
(39) Zhao, Y.; Truhlar, D. G. The M06 Suite of Density Functionals for Main Group Thermochemistry, Thermochemical Kinetics, Noncovalent Interactions, Excited States, and Transition Elements: Two New Functionals and Systematic Testing of Four M06-Class Functionals and 12 Other Functionals. *Theor. Chem. Acc.* **2008**, *120* (1−3), 215−241.
(40) Dinda, S.; Chiu, C.-C.; Genest, A.; Rösch, N. Evaluation of Density Functionals for Elementary Steps of Selective Oxidation Reactions. *Comput. Theor. Chem.* **2017**, *1101*, 36−45.
(41) Goncalves, T. J.; Plessow, P. N.; Studt, F. On the Accuracy of Density Functional Theory in Zeolite Catalysis. *ChemCatChem* **2019**, *11* (17), 4368−4376.
(42) Goerigk, L.; Grimme, S. A Thorough Benchmark of Density Functional Methods for General Main Group Thermochemistry, Kinetics, and Noncovalent Interactions. *Phys. Chem. Chem. Phys.* **2011**, *13* (14), 6670.
(43) Grimme, S.; Antony, J.; Ehrlich, S.; Krieg, H. A Consistent and Accurate *Ab Initio* Parametrization of Density Functional Dispersion Correction (DFT-D) for the 94 Elements H-Pu. *J. Chem. Phys.* **2010**, *132* (15), 154104.
(44) Busch, M.; Fabrizio, A.; Luber, S.; Hutter, J.; Corminboeuf, C. Exploring the Limitation of Molecular Water Oxidation Catalysts. *J. Phys. Chem. C* **2018**, *122* (23), 12404−12412.
(45) Okazaki, I.; Sato, F.; Yoshihiro, T.; Ueno, T.; Kashiwagi, H. Development of a Restricted Open Shell Kohn−Sham Program and Its Application to a Model Heme Complex. *J. Mol. Struct.: THEOCHEM* **1998**, *451* (1−2), 109−119.
(46) Kresse, G.; Hafner, J. *Ab Initio* Molecular Dynamics for Liquid Metals. *Phys. Rev. B* **1993**, *47* (1), 558−561.
(47) Kresse, G.; Furthmüller, J. Efficient Iterative Schemes for *Ab Initio* Total-Energy Calculations Using a Plane-Wave Basis Set. *Phys. Rev. B* **1996**, *54* (16), 11169−11186.
(48) Kresse, G.; Furthmüller, J. Efficiency of Ab-Initio Total Energy Calculations for Metals and Semiconductors Using a Plane-Wave Basis Set. *Comput. Mater. Sci.* **1996**, *6* (1), 15−50.
(49) Govindasamy, A.; Muthukumar, K.; Yu, J.; Xu, Y.; Guliants, V. V. Adsorption of Propane, Isopropyl, and Hydrogen on Cluster Models of the M1 Phase of Mo−V−Te−Nb−O Mixed Metal Oxide Catalyst. *J. Phys. Chem. C* **2010**, *114* (10), 4544−4549.
(50) Yu, J.; Xu, Y.; Guliants, V. V. Propane Ammoxidation over Mo−V−Te−Nb−O M1 Phase: Density Functional Theory Study of Propane Oxidative Dehydrogenation Steps. *Catal. Today* **2014**, *238*, 28−34.
(51) Johnson, R. D. *Computational Chemistry Comparison and Benchmark Database, NIST Standard Reference Database 101*; NIST, 2002; ..
(52) Latimer, A. A.; Kulkarni, A. R.; Aljama, H.; Montoya, J. H.; Yoo, J. S.; Tsai, C.; Abild-Pedersen, F.; Studt, F.; Nørskov, J. K. Understanding Trends in C−H Bond Activation in Heterogeneous Catalysis. *Nat. Mater.* **2017**, *16* (2), 225−229.
(53) Miyajima, M.; Watanabe, Y.; Nakano, H. Relativistic Quasidegenerate Perturbation Theory with Four-Component General Multiconfiguration Reference Functions. *J. Chem. Phys.* **2006**, *124* (4), 044101.
(54) Nakano, H.; Uchiyama, R.; Hirao, K. Quasi-degenerate Perturbation Theory with *General* Multiconfiguration Self-consistent Field Reference Functions. *J. Comput. Chem.* **2002**, *23* (12), 1166−1175.
(55) Alexopoulos, K.; Reyniers, M.-F.; Marin, G. B. Reaction Path Analysis of Propane Selective Oxidation over V_2O_5 and V_2O_5/TiO_2. *J. Catal.* **2012**, *289*, 127−139.
(56) Kozuch, S.; Shaik, S. How to Conceptualize Catalytic Cycles? The Energetic Span Model. *Acc. Chem. Res.* **2011**, *44* (2), 101−110.
(57) Liu, Y.; Annamalai, L.; Deshlahra, P. Effects of Lattice O Atom Coordination and Pore Confinement on Selectivity Limitations for Ethane Oxidative Dehydrogenation Catalyzed by Vanadium-Oxo Species. *J. Phys. Chem. C* **2019**, *123* (46), 28168−28191.
(58) Annamalai, L.; Ezenwa, S.; Dang, Y.; Tan, H.; Suib, S. L.; Deshlahra, P. Comparison of Structural and Catalytic Properties of

Monometallic Mo and V Oxides and M1 Phase Mixed Oxides for Oxidative Dehydrogenation. *Catal. Today* **2021**, *368*, 28−45.
(59) Naumann d'Alnoncourt, R.; Kolen'ko, Y. V.; Schlogl, R.; Trunschke, A. A New Way of Probing Reaction Networks: Analyzing Multidimensional Parameter Space. *Comb. Chem. High Throughput Screening* **2012**, *15* (2), 161−169.
(60) Kubas, A.; Noak, J.; Trunschke, A.; Schlögl, R.; Neese, F.; Maganas, D. A Combined Experimental and Theoretical Spectroscopic Protocol for Determination of the Structure of Heterogeneous Catalysts: Developing the Information Content of the Resonance Raman Spectra of M1MoVO$_x$. *Chem. Sci.* **2017**, *8* (9), 6338−6353.
(61) Gaffney, A. M.; An, Q.; Goddard, W. A.; Diao, W.; Glazoff, M. V. Toward Concurrent Engineering of the M1-Based Catalytic Systems for Oxidative Dehydrogenation (ODH) of Alkanes. *Top. Catal.* **2020**, *63* (19−20), 1667−1681.
(62) Goddard, W. A. Quantum Mechanics Based Mechanisms for Selective Activation of Hydrocarbons by Mixed Metal Oxide Heterogeneous Catalysts − A Tribute to Robert Grasselli. *Catal. Today* **2021**, *363*, 3−9.
(63) Zhu, Y.; Jensen, E.; Sushko, P. V.; Kovarik, L.; Sanchez-Sanchez, M.; Lercher, J. A.; Melzer, D.; Ophus, C.; Browning, N. D. The Merits of In Situ Environmental STEM for the Study of Complex Oxide Catalysts at Work. *Microsc. Microanal.* **2018**, *24* (S1), 238−239.
(64) Melzer, D.; Mestl, G.; Wanninger, K.; Jentys, A.; Sanchez-Sanchez, M.; Lercher, J. A. On the Promoting Effects of Te and Nb in the Activity and Selectivity of M1MoV-Oxides for Ethane Oxidative Dehydrogenation. *Top. Catal.* **2020**, *63* (19−20), 1754−1764.
(65) Zhu, Y.; Sushko, P. V.; Melzer, D.; Jensen, E.; Kovarik, L.; Ophus, C.; Sanchez-Sanchez, M.; Lercher, J. A.; Browning, N. D. Formation of Oxygen Radical Sites on MoVNbTeOx by Cooperative Electron Redistribution. *J. Am. Chem. Soc.* **2017**, *139* (36), 12342−12345.
(66) Melzer, D.; Mestl, G.; Wanninger, K.; Zhu, Y.; Browning, N. D.; Sanchez-Sanchez, M.; Lercher, J. A. Design and Synthesis of Highly Active MoVTeNb-Oxides for Ethane Oxidative Dehydrogenation. *Nat. Commun.* **2019**, *10* (1), 4012.
(67) Melzer, D.; Xu, P.; Hartmann, D.; Zhu, Y.; Browning, N. D.; Sanchez-Sanchez, M.; Lercher, J. A. Atomic-Scale Determination of Active Facets on the MoVTeNb Oxide M1 Phase and Their Intrinsic Catalytic Activity for Ethane Oxidative Dehydrogenation. *Angew. Chem., Int. Ed.* **2016**, *55* (31), 8873−8877.
(68) Li, W.; Fjermestad, T.; Genest, A.; Rösch, N. How the Distribution of Reduced Vanadium Centers Affects Structure and Stability of the MoVO$_x$ Material. *Catal. Sci. Technol.* **2018**, *8* (10), 2654−2660.
(69) Arce-Ramos, J. M.; Rugg, G.; Genest, A.; Rösch, N. Probing the Positions of TeO Moieties in the Channels of the MoVNbTeO M1 Catalyst: A Density Functional Theory Model Study. *Catal. Lett.* **2021**, *151* (10), 2884−2893.
(70) Fjermestad, T.; Li, W.-Q.; Genest, A.; Rösch, N. Configurations of V^{4+} Centers in the MoVO Catalyst Material. A Systematic Stability Analysis of DFT Results. *SN Appl. Sci.* **2020**, *2* (11), 1909.
(71) Fjermestad, T.; Li, W.-Q.; Rugg, G.; Ishida, S.; Okuno, M.; Sagi, K.; Genest, A.; Rösch, N. Acrolein Oxidation to Acrylic Acid over the MoVOx Material. Insights from DFT Modeling. *Appl. Catal., A* **2018**, *565*, 68−75.
(72) Pyrz, W. D.; Blom, D. A.; Vogt, T.; Buttrey, D. J. Direct Imaging of the MoVTeNbO M1 Phase Using An Aberration-Corrected High-Resolution Scanning Transmission Electron Microscope. *Angew. Chem., Int. Ed.* **2008**, *47* (15), 2788−2791.
(73) Blom, D. A.; Vogt, T. Multi-Slice Frozen Phonon Simulations of High-Angle Annular Dark Field Scanning Transmission Electron Microscopy Images of the Structurally and Compositionally Complex Mo−V−Nb−Te Oxide Catalyst. *Adv. Struct. Chem. Imaging* **2018**, *4* (1), 9.
(74) Aouine, M.; Epicier, T.; Millet, J.-M. M. In Situ Environmental STEM Study of the MoVTe Oxide M1 Phase Catalysts for Ethane Oxidative Dehydrogenation. *ACS Catal.* **2016**, *6* (7), 4775−4781.
(75) Kardash, T. Y.; Lazareva, E. V.; Svintsitskiy, D. A.; Ishchenko, A. V.; Bondareva, V. M.; Neder, R. B. The Evolution of the M1 Local Structure during Preparation of VMoNbT eOCatalysts for Ethane Oxidative Dehydrogenation to Ethylene. *RSC Adv.* **2018**, *8* (63), 35903−35916.
(76) Pyrz, W. D.; Blom, D. A.; Shiju, N. R.; Guliants, V. V.; Vogt, T.; Buttrey, D. J. Using Aberration-Corrected STEM Imaging to Explore Chemical and Structural Variations in the M1 Phase of the MoVNbT eO Oxidation Catalyst. *J. Phys. Chem .C* **2008**, *112* (27), 10043−10049.
(77) Studt, F. Grand Challenges in Computational Catalysis. *Front. Catal.* **2021**, *1*, No. 658965.